Catalytic Growth of Silicon Nanowires Assisted by Laser Ablation

Yi-Han Yang, Sheng-Jia Wu, Hui-Shan Chiu, Ping-I Lin, and Yit-Tsong Chen*

Department of Chemistry, National Taiwan University, Taipei 106, Taiwan, ROC, and Institute of Atomic and Molecular Sciences, Academia Sinica, P.O. Box 23-166, Taipei 106, Taiwan, ROC

Silicon nanowires (SiNWs, diameter $\geq$ 5 nm, and length $\sim \mu$m) have been fabricated with metal- and SiO_2-catalyses assisted by laser ablation. In the catalytic growth of single-crystalline SiNWs by pure metal catalysts (Fe, Ru, and Pr), Si {111} is found to be the most stable plane and wire growth axis is along ⟨111⟩. The growth mechanism follows a vapor−liquid−solid process, and the synthesized SiNWs typically have metal-tips composed of metal and Si, such as $FeSi_2$, $RuSi_3$, and $PrSi_4$, respectively. In sharp contrast, a crystalline growth axis of ⟨111⟩ and a wire growth axis of ⟨112⟩ are the result in the SiNWs catalyzed by SiO_2. Besides, the SiO_2-catalytic SiNWs generally have no tips at the wire ends. Distinctive growth mechanisms resulting from metal- and SiO_2-catalyses will be discussed. Pressure effect on the longitudinal and transverse growing rates in the fabrication of SiNWs has been examined.

1. Introduction

The optical and electrical properties of semiconductor-based nanostructures have recently stimulated tremendous research interest. A distinctive feature for semiconductor-based nanostructures relative to bulky material is the well-known quantum confinement effect owing to the reduced size and/or dimensionality.[1−3] Silicon (Si) is an important semiconductor material with its contemporary microelectronic technology being one of the greatest successes for the past century. Nevertheless, there is still room for improvement in the applications of Si-based optoelectronic devices. For instance, Si is an indirect band-gap ($\sim$1.1 eV) material with a small exciton binding energy ($\sim$15 meV), and does not emit visible light. For this reason, a great deal of effort has been made lately to fabricate lower dimensional nanostructures,[4−6] such as quantum wells, nanowires, and quantum dots,[2,3] in which the motion of charge carriers is confined, causing an increase of the band gap[7] and/or a transformation of the electronic band structure from an indirect band gap to a direct one.

The advance of nanotechnology has led to a way to fabricate semiconductor materials from micro- to nanometers in size. Among other developments, more and more syntheses for one-dimensional nanowires have been accomplished. For Si, in particular, intensive research of one-dimensional nanowires and their corresponding optical and electrical properties has been done by several groups, such as Lee,[8−20] Lieber,[21−26] and Yu.[12,13,27−37] In the research studies approached by these groups, the wirelike crystalline nanostructures of Si were often fabricated via vapor−liquid−solid (VLS) growth,[38,39] in which a liquid cluster of metal-catalyst provides energetically favored sites for the absorption/adsorption of gas-phase reactants. The sizes of the catalysts are considered to be responsible for diameters of the resultant silicon nanowires (SiNWs). Based on this correspondence, the application of laser ablation to vaporize a target sample of bulky Si, mixed with metal catalyst, and to form small

sizes of nanoclusters in the initial VLS process is a unique and quite powerful method in the fabrication of one-dimensional SiNWs.

Different from the SiNWs catalyzed by metal nanoclusters via the VLS mechanism, another process for the nucleation and growth of SiNWs, catalyzed by silicon dioxide (SiO_2), has been reported by Lee and co-workers in laser ablation[8,12−16] as well as in thermal evaporation.[9−10,17−20] In this work, we will investigate the catalytic roles of different metal catalysts (Fe, Ru, Pr, $RuCl_3$, and Pr_6O_{11}) and SiO_2 in the syntheses of SiNWs assisted by laser ablation. From these comparisons, we have tried to discern the growth mechanism via SiO_2-catalysis from that via the VLS in traditional metal-catalytic processes. Differences in the crystalline and wire growth axes of SiNWs have been examined for the SiO_2- and metal-catalytic SiNWs.

2. Experiment

The apparatus used in our catalytic-growth experiments assisted by laser ablation is depicted in Figure 1. An evacuated alumina tube, placed inside a furnace, contains a target sample of Si powder (Acros, 325 mesh, 99+%) and metal catalyst. We have used iron (Fe) powder (Prochem, 325 mesh, 99.9%), ruthenium (Ru) powder (Strem, 99.9%), praseodymium (Pr) powder (Strem, 40 mesh, 99.9% REO), ruthenium chloride ($RuCl_3$) powder (Strem, anhydrous, 47.44% Ru), and praseodymium oxide (Pr_6O_{11}) powder (Strem, 99.9% Pr), respectively, as metal catalysts. Alternatively, SiO_2 (Aldrich, 325 mesh, 99.6%) was regarded as another supplying source for Si, and had also been introduced in the target sample. Totally, we have carried out six experiments, including Si + Fe, Si + Ru, Si + Pr, Si + SiO_2 + Fe, Si + SiO_2 + $RuCl_3$, and Si + SiO_2 + Pr_6O_{11}, respectively, as reacting ingredients. In the experiments without SiO_2 in the target sample, Si powder and metal catalyst (Fe, Pr, or Ru) were mixed with a weight ratio of 90:10%. When SiO_2 was used in the growth of SiNWs, the weight ratio of Si/SiO_2/metal compound (Fe, Pr_6O_{11}, or $RuCl_3$) was typically 45:45:10%.

The sample mixture was pressed into a pellet, placed in a crucible/quartz holder, and located in the center of the alumina

* Author to whom all correspondence should be addressed at Institute of Atomic and Molecular Sciences, Academia Sinica, P.O. Box 23-166, Taipei 106, Taiwan. Fax: +886-2-2362-0200. E-mail: ytchen@pub.iams.sinica.edu.tw.
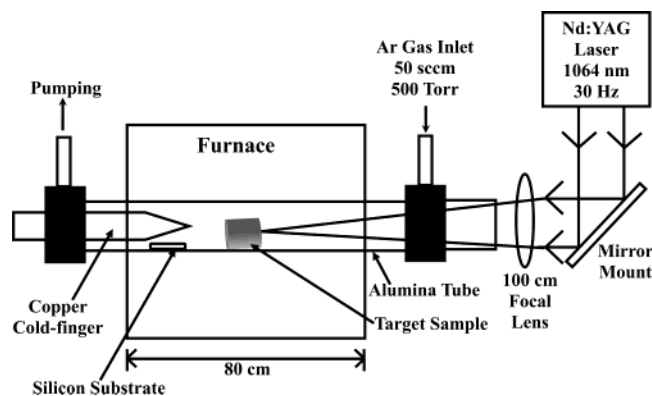
Catalytic Growth of Silicon Nanowires

J. Phys. Chem. B, Vol. 108, No. 3, 2004 **847**

Figure 1. Apparatus for the catalytic-growth experiments of SiNWs assisted by laser ablation.

tube across the heating furnace (Figure 1). At one end of the alumina tube, an S1-UV window was attached for the pass of the laser beam; at the other, a water-cooling copper-finger and a Si-substrate were prepared for the collection of synthesized SiNWs. Before elevating the temperature, the alumina tube was evacuated, and then heated to 850 °C for the tube-wall degassing for 2 h. As such, impurities coated on the target sample can also be removed. After degassing, temperature was elevated gradually to reach a point depending on the catalyst used, e.g., a eutectic temperature of $FeSi_2$ at 1207 °C if Fe was employed as a catalyst, or 1212 °C when Pr was used. Argon (Ar) as a carrier gas with a typical total pressure of ∼500 Torr and a flow rate of 50 sccm was maintained throughout the experiment.

When the gas flow reaches steady, a pulsed Nd:YAG laser (Spectra Physics, GCR-190) with 1064 nm wavelength, 30 Hz repetition rate, and ∼70 mJ/pulse was ignited to ablate the target sample. The laser beam passing through a lens of 100-cm focal length was confined into 1.5 mm in diameter on the target sample. A computer programmed alignment-control for the mirror-mount has been designed to guide the laser beam moving from one spot on the target sample to another during the ablation process. As such, the laser could ablate fresh sample-spots in the course of experiment. The reaction time ranges from a half to a few hours. Finally, a dark yellow-colored spongelike product was collected from the cold surface of the copper-finger, the Si-substrate, and the inside wall of the alumina tube as well.

Morphologies of as-synthesized SiNWs have been taken from a scanning electron microscope (SEM) and a transmission electron microscope (TEM). The SEM morphologies of SiNWs were performed in (1) JEOL JSM-6300 SEM with Link EXL II EDX, (2) Hitachi S-800 Field Emission SEM, and (3) LEO l530 Field Emission Gun SEM, and Energy Dispersive Spectrometer (FEG-SEM + EDS). The TEM images of SiNWs were carried out by JEOL JEM-1200EX II TEM at 80 kV and Hitachi H-7100 TEM at 75 kV. High-resolution transmission electron microscope (HRTEM) images of SiNWs were obtained by a Philips Tecnai F30 Field Emission Gun TEM (FEG-TEM) with an EDAX Energy Dispersive X-ray Spectrometer at 300 kV, JEOL JEM-2010 Analytical TEM at 200 kV, and JEOL JEM-4000EX HRTEM at 400 kV.

3. Results and Discussion

3.1. Nanowire Synthesis. *Catalyses by Fe and SiO_2.* In the fabrication of SiNWs using Fe as a catalyst, the target sample for laser ablation is composed of Si/Fe = 90:10% (weight ratio). Alternatively, SiO_2 was supposed to be another supplying source for Si. We also used samples of Si/SiO_2/Fe = 45:45:10% as reactants. The morphological contrasts in SEM, TEM, and
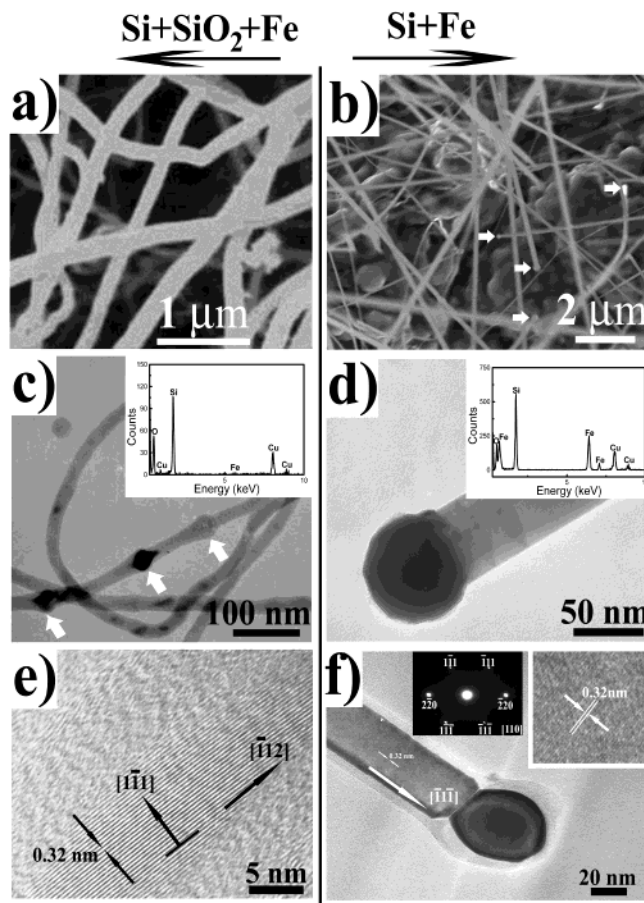

Figure 2. (a) SEM morphology of the SiNWs fabricated from Si + SiO_2 + Fe, where the diameters of SiNWs range from 50 to 300 nm and the lengths are micrometers. (b) SEM morphology of the SiNWs catalyzed by Fe only, where the SiNWs are quite uniform. Parts of metal-tips at the SiNWs are marked by arrows. (c) TEM image for the SiO_2-catalytic SiNWs of ∼25 nm diameter. The beadlike nanoparticles/nanoclusters (marked by arrows) comprise Si, O, (molar ratio, Si/O = 1:2), Cu (background of the Cu grid for TEM measurement), and a negligible amount of Fe as revealed by an EDS analysis (inset). (d) TEM image of an Fe-catalytic SiNW. The composition of the tip attached to the wire is $FeSi_2$ as determined by EDS (inset). (e) HRTEM image shows the ($1\bar{1}1$) crystalline plane with *d*-spacing of 0.32 nm in a SiO_2-catalytic SiNW. The [$1\bar{1}1$] crystalline growth axis is perpendicular to the wire growth axis of [$\bar{1}12$]. The crystalline Si core and amorphous SiO_x sheath are also visualized. (f) HRTEM morphology for Fe-catalytic SiNW. From the ED pattern (upper-left inset) recorded along the [110] zone axis, the wire grows along the [$\bar{1}1\bar{1}$] direction and ($1\bar{1}\bar{1}$) lattice planes are of 0.32-nm *d*-spacing (upper-right inset).

HRTEM between the SiNWs synthesized by Si + SiO_2 + Fe and those by Si + Fe are shown, respectively, in the left and right sides of Figure 2.

Figure 2a shows the SEM image of SiNWs resulting from the reaction of Si + SiO_2 + Fe at 500 Torr of Ar carrier pressure, where the diameters of SiNWs range from 50 to 300 nm and the lengths are expressed in micrometers. By comparison, Fe-catalytic SiNWs fabricated without SiO_2 in the target sample are shown in Figure 2b. Without SiO_2, the synthesized SiNWs possess a sharper distribution in wire-diameter. Metal-tips have also been found at the fabricated SiNWs, marked in part by arrows in Figure 2b, indicating a catalytic growth following the VLS mechanism.

TEM morphology in Figure 2c shows that the majority of the SiNWs, fabricated from Si + SiO_2 + Fe, contain bead-(marked by arrows in Figure 2c) and wire-like nanostructures where the beadlike nanoparticles/nanoclusters are embedded in

TABLE 1: Growth Direction, Composition, Crystallization, and Dimension of Catalytically Synthesized SiNWs

	reacting ingredients					
	Si + Fe	Si + Ru	Si + Pr	S i+ SiO_2 + Fe[a]	Si + SiO_2 + $RuCl_3$[b]	Si+SiO_2 + Pr_6O_{11}[c]
crystalline growth axis	$[\bar{1}\bar{1}\bar{1}]$	$[1\bar{1}\bar{1}]$	$[\bar{1}\bar{1}\bar{1}]$	$[1\bar{1}\bar{1}]$	$[1\bar{1}\bar{1}]$	$[1\bar{1}\bar{1}]$
wire growth axis	$[\bar{1}\bar{1}\bar{1}]$	$[1\bar{1}\bar{1}]$	$[\bar{1}\bar{1}\bar{1}]$	$[\bar{1}12]$	$[\bar{1}12]$	$[\bar{1}12]$
tip composition	$FeSi_2$	$RuSi_3$	$PrSi_4$	SiO_x	SiO_x	SiO_x
wire crystallization	single	single	single + poly	single	single	single
Si core diameter	~36 nm	~5 nm	~16 nm	~8 nm	~5 nm	~15 nm
SiO_x sheath thickness	~5 nm	~9 nm	~3 nm	~9 nm	~10 nm	~5 nm

[a] Ratio of 92:8% is found for the fabricated SiNWs with $[1\bar{1}\bar{1}]$ crystalline growth axis and $[\bar{1}12]$ wire growth axis catalyzed by SiO_2 to those with $[\bar{1}\bar{1}\bar{1}]$ crystalline growth axis and $[\bar{1}\bar{1}\bar{1}]$ wire growth axis catalyzed by Fe. This column represents the major product of SiO_2-catalytic SiNWs. [b] Ratio of 92.3:7.7% is found for the fabricated SiNWs with $[1\bar{1}\bar{1}]$ crystalline growth axis and $[\bar{1}12]$ wire growth axis catalyzed by SiO_2 to those with $[1\bar{1}\bar{1}]$ crystalline growth axis and $[1\bar{1}\bar{1}]$ wire growth axis catalyzed by $RuCl_3$. This column represents the major product of SiO_2-catalytic SiNWs. [c] Ratio of 95.5:4.5% is found for the fabricated SiNWs with $[1\bar{1}\bar{1}]$ crystalline growth axis and $[\bar{1}12]$ wire growth axis catalyzed by SiO_2 to those with $[\bar{1}\bar{1}\bar{1}]$ crystalline growth axis and $[\bar{1}\bar{1}\bar{1}]$ wire growth axis catalyzed by Pr_6O_{11}. This column represents the major product of SiO_2-catalytic SiNWs.

the nanowires or bridging sequential wire-sections. To understand details about the growth mechanism, energy dispersive spectroscopy (EDS) was taken to analyze the chemical composition of the fabricated SiNWs. The inset of Figure 2c shows an EDS for the beadlike nanoparticles/nanoclusters, which comprise Si, O, (molar ratio, Si/O = 1:2), Cu (background of the Cu grid for TEM measurement), and a negligible amount of Fe. The absence of Fe in the beadlike nanoparticles/ nanoclusters indicates that the growing is unlike a general process complying with an ordinary VLS mechanism, where metal-catalyst is often found to appear at the tip, root, or middle of synthesized nanowires. In sharp contrast, SiNWs synthesized from Si + Fe have distinct Fe-head and Si-wire-body as shown in Figure 2d. An EDS analysis (inset of Figure 2d) reveals that the tip of the SiNW is mainly composed of $FeSi_2$. This composition agrees very well with the phase diagram of Si−Fe binary elements under the present experimental condition. In addition to the distinctive structures resulting from the presence/absence of SiO_2, diverse morphologies such as belt-, whisker-, and fishbone-like nanostructures are also found in the Fe-catalytic SiNWs (not shown).

An HRTEM image gives the microstructures about the inner core and outer sheath of the SiNWs fabricated from Si + SiO_2 + Fe (Figure 2e), which depicts an outer sheath of ~9 nm thickness and a crystalline core of ~8 nm diameter. From the HRTEM image in Figure 2e, the crystalline growth axis of the SiNWs is along the $[1\bar{1}\bar{1}]$ direction with d-spacing of 0.32 nm. The wire growth axis directs to $[\bar{1}12]$, which is determined by an electron diffraction (ED) measurement (not shown). The $(1\bar{1}\bar{1})$ crystalline planes of SiNWs are parallel to the $[\bar{1}12]$ wire growth axis, as can be seen in Figure 2e and tabulated in Table 1. It is noted that the majority (92%) of the SiNWs fabricated from Si + SiO_2 + Fe (weight ratio = 45:45:10%) contain wire growth axis along $[\bar{1}12]$ and the minority (8%) of them orient at $[1\bar{1}\bar{1}]$ (Table 1). On the other hand, wire growth axis of the SiNWs fabricated from Si + Fe is all along $[\bar{1}\bar{1}\bar{1}]$(Figure 2f), indicating that the $(\bar{1}\bar{1}\bar{1})$ crystalline planes are perpendicular to the wire growth axis.

The distinctive wire growth axes of $[\bar{1}12]$ and $[\bar{1}1\bar{1}]$ in the fabricated SiNWs (Figures 2e and 2f), respectively, from Si + SiO_2 + Fe and Si + Fe, indicate that different mechanisms have been followed with or without SiO_2 in the reactant ingredients. In an earlier study by Lee and co-workers,[8,9] SiO_2 was put forward as a catalyst, and the SiO_2-containing reaction to fabricate SiNWs does not comply with an ordinary VLS mechanism. While the catalytic role of SiO_2 will be discussed later in section 3.2, competition between SiO_2 and Fe as catalysts in the fabrication of SiNWs has been observed in the present experiment. In the fabrication from Si + SiO_2 + Fe, the yield ratio of 92:8% (Table 1) for the SiNWs of ⟨112⟩ and ⟨111⟩ wire growth axes resulting from the catalyses of SiO_2 and Fe, respectively, is out of proportion to the weight ratio of SiO_2/Fe = 45:10% in the initial target-sample. This abnormal product/ reactant ratio may suggest an easier reaction, either thermodynamically or kinetically, for Si + SiO_2 than for Si + Fe in the fabrications of SiNWs.

Despite the different wire growth axes, the SiNWs catalyzed by pure Fe (Figure 2f) have the same Si-core and SiO_x-sheath nanostructure as those catalyzed by SiO_2 (Figure 2e). The oxygen could be due to the relatively low vacuum (~1 mTorr) in the reaction tube. The Fe-catalytic SiNW (Figure 2f) has a crystalline Si core of ~36 nm in diameter and an amorphous SiO_x outer-layer of ~5 nm in thickness. The 0.32 nm crystalline spacing observed in the inner core of Fe-catalytic SiNWs (upper-right inset of Figure 2f) corresponds to the d-spacing of Si {111} lattice planes. In the Fe-catalytic growth of SiNWs, the Si {111} crystalline planes are reported to be most stable.[27] The ED pattern from the inner core of SiNW (upper-left inset of Figure 2f) indicates that the SiNW has a $[1\bar{1}\bar{1}]$ wire growth axis perpendicular to the $(\bar{1}1\bar{1})$ lattice planes (Table 1). The wire extruding from the $FeSi_2$-tip and growing along the ⟨111⟩ direction (Figures 2d and 2f) provides clear evidence for the VLS mechanism in the SiNW synthesis. This result is consistent with previous studies by Wagner[39] and Lieber and co-workers[21] that the crystalline growth axis of ⟨111⟩ is most favorable in the metal-catalytic fabrication of SiNWs via VLS processes. The crystalline growth axis, wire growth axis, tip composition, wire crystallization, Si core diameter, and SiO_x sheath thickness for the Fe- and SiO_2-catalytic SiNWs are listed in Table 1 for comparison.

Catalyses by Ru and SiO_2. We have also synthesized SiNWs with samples of Si + SiO_2 + $RuCl_3$ (45:45:10%) and Si + Ru (90:10%), respectively, and conveyed the SEM, TEM, HRTEM, ED, and EDS of these fabricated SiNWs in the upper and lower parts of Figure 3. Like what we discussed earlier, when both $RuCl_3$ and SiO_2 coexist as catalysts, SiO_2 plays a dominant catalytic role over $RuCl_3$ that could partly result from its prevailing abundance in the reacting sample. In general, the SiNWs fabricated from the mixture of Si + SiO_2 + $RuCl_3$ have ~10−50 nm diameters, appreciable wire-length, and no apparent metal-tips were found to attach at the ends of SiNWs (Figure 3a). For detailed investigation, the TEM image of the SiO_2-catalytic SiNWs shown in Figure 3b further demonstrates uniformity in the diameters (12−15 nm) of as-grown SiNWs.

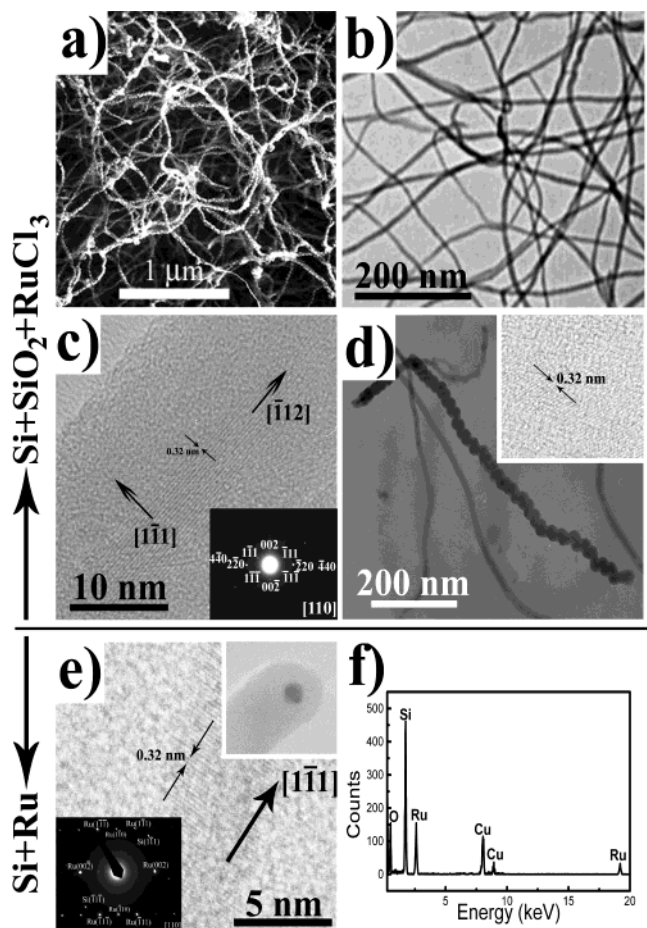The SiO_2-catalytic SiNWs, again, have core-sheath microstructure, as can be seen in HRTEM morphology (Figure 3c),

Catalytic Growth of Silicon Nanowires

J. Phys. Chem. B, Vol. 108, No. 3, 2004 **849**

Figure 3. (a) SEM morphology of the SiNWs fabricated from Si + SiO_2 + $RuCl_3$, where the SiNWs have a sharp diameter distribution at ∼35 nm and tens of micrometers in length. (b) TEM morphology of SiO_2-catalytic SiNWs with diameters at 12−15 nm. (c) HRTEM image of the SiO_2-catalytic SiNW shows the crystalline Si core of ∼5 nm diameter, [1$\bar{1}$1] crystalline growth axis with *d*-spacing of 0.32 nm, and [$\bar{1}$12] wire growth axis. (d) TEM morphology depicts a coil-like SiNW of ∼30 helical pitches, ∼30 nm wire-diameter, ∼32 nm pitch-length, and ∼50 nm coil-diameter. The coiled SiNW is single crystalline with the growing axis normal to the Si {111} lattice planes (0.32 nm *d*-spacing in the inset). (e) HRTEM image of a Ru-catalytic SiNW with an ultrathin Si core of ∼5 nm diameter and a very thick SiO_x amorphous outer-shell (upper-right inset). Crystalline Si (1$\bar{1}$1) planes with 0.32 nm *d*-spacing are perpendicular to the [1$\bar{1}$1] wire growth axis. An ED pattern (lower-left inset), recorded along the [110] zone axis, reveals the crystalline structures of Si and Ru for the tip of the wire. (f) EDS spectrum for the tip of the Ru-catalytic SiNW shown in the upper-right inset of 3e. Except for the O and Cu signals belonging to the background, the composition of the wire-tip is $RuSi_3$.

where the Si core (∼5 nm in diameter) is distinctly smaller than the outer amorphous SiO_x sheath (∼10 nm). The small diameter of the Si core is comparable to those SiNWs fabricated from zeolite.[20] From the HRTEM in Figure 3c, the (1$\bar{1}$1) lattice fringes with *d*-spacing of 0.32 nm is observed. The wire growth axis, along the [$\bar{1}$12] direction, can be identified from the ED pattern as depicted in the inset of Figure 3c. These SiNWs catalyzed by SiO_2 have almost no contamination from the metallic catalyst according to EDS analysis (not shown); neither has any metallic tip been found in the wires. This outcome again suggests that SiO_2 plays a dominant catalytic role in the growth of SiNWs from Si + SiO_2 + $RuCl_3$ similar to the previous case of Si + SiO_2 + Fe. The fabricated SiNWs also have ⟨112⟩ and ⟨111⟩ wire growth axes at a ratio of 92.3:7.7%, once more, indicating the competition of catalytic roles between SiO_2 and

$RuCl_3$ in the reaction. It is noteworthy that $RuCl_3$ decomposes into Ru and Cl_2 at high temperature,[40] and the reduced Ru, as a catalyst subsequently, is responsible for the fabricated SiNWs of ⟨111⟩ wire growth axis.

For Ru-catalytic SiNWs, the SEM morphology is quite similar to that of SiO_2-catalytic SiNWs (Figure 3a). Figure 3e shows a typical HRTEM image for the wire-body of a Ru-catalytic SiNW with a [1$\bar{1}$1] wire growth axis perpendicular to the Si (1$\bar{1}$1) crystalline planes (d = 0.32 nm). The SiNW contains a metal-tip as depicted in the upper-right inset of Figure 3e. The tip is composed of $RuSi_3$ revealed from an EDS measurement (Figure 3f). It is interesting to note that the Ru-catalytic SiNWs contain a heavy amorphous SiO_x outer-shell around the $RuSi_3$-tip. The SiNWs have a very thin crystalline Si core (only ∼5 nm in diameter) and relatively thick amorphous outer-sheath (∼9 nm in thickness) (Figure 3e and Table 1). The thick SiO_x sheath is owing to the higher oxidation potential for Ru than that for Si (despite the quite easy oxidation ability for Si itself).[41] Moreover, an ED pattern for the wire-tip recorded along the [110] zone axis (lower-left inset of Figure 3e) provides information about the tip-composition of Si and Ru. The growth direction, composition, crystallization, and dimension of Ru- and SiO_2-catalytic SiNWs are also tabulated in Table 1.

In addition to the filamentary nanowires, some interesting coil-like structure is also present in the products fabricated from Si + SiO_2 + $RuCl_3$ (Figure 3d). The TEM image in Figure 3d shows that the coiled SiNW is of ∼30 helical pitches, ∼30 nm wire-diameter, ∼32 nm pitch-length, and ∼50 nm coil-diameter. From HRTEM (inset of Figure 3d), the coiled SiNW is revealed to be single crystalline with a growing axis normal to the Si {111} lattice planes (0.32 nm *d*-spacing). The Si bonding in the helical SiNWs is an interesting subject to be studied in future. Referring to the very recently discovered bent Si=Si=Si structure in trisilaallene containing a formally sp-hybridized Si atom,[42] the structural characterization of Si atoms in the presently observed helical SiNWs will be very intriguing to be unraveled.

Catalyses by Pr and SiO_2. Microscopic images, ED, and EDS analyses for the SiNWs fabricated from Si + SiO_2 + Pr_6O_{11} and Si + Pr samples are shown in the upper and lower parts of Figure 4, respectively. Once more, the synthesized SiNWs from Si + SiO_2 + Pr_6O_{11} are catalyzed dominantly by SiO_2 (95.5%) and lesser by Pr_6O_{11} (4.5%) (Table 1). In addition to the normal SiNWs (SEM morphology in Figure 4a), helical belts (inset of Figure 4a) have also been synthesized from Si + SiO_2 + Pr_6O_{11}. The dimensions for the helical belts are ∼60 μm pitch-length, ∼40 μm belt-width, and ∼3 μm belt-thickness. TEM morphology of the SiO_2-catalytic SiNWs (Figure 4b) shows a narrow distribution of wire diameter at ∼30 nm. The inset of Figure 4b gives a selected-area electron diffraction (SAED) pattern for the SiNW (marked by an arrow in Figure 4b) with the electron beam along the [110] zone axis. While the SAED in Figure 4b shows a single crystallite for the SiNW, plane defects could occasionally be observed in TEM images (not shown). The crystalline structure of SiNWs can further be visualized in the HRTEM image of Figure 4c.

From the HRTEM lattice image of SiO_2-catalytic SiNWs (Figure 4c), crystalline Si (1$\bar{1}$1) planes are observed with *d*-spacing of 0.32 nm, and wire growth axis orients to the [$\bar{1}$12] direction. Moreover, this SiNW has the crystalline-core and amorphous-sheath structure similar to those SiNWs catalyzed by SiO_2 discussed earlier. Analysis for the SAED pattern (inset of Figure 4c), taken from a spot in the wire-core, shows the coexistence of the {111}, {220}, and {311} lattice plane
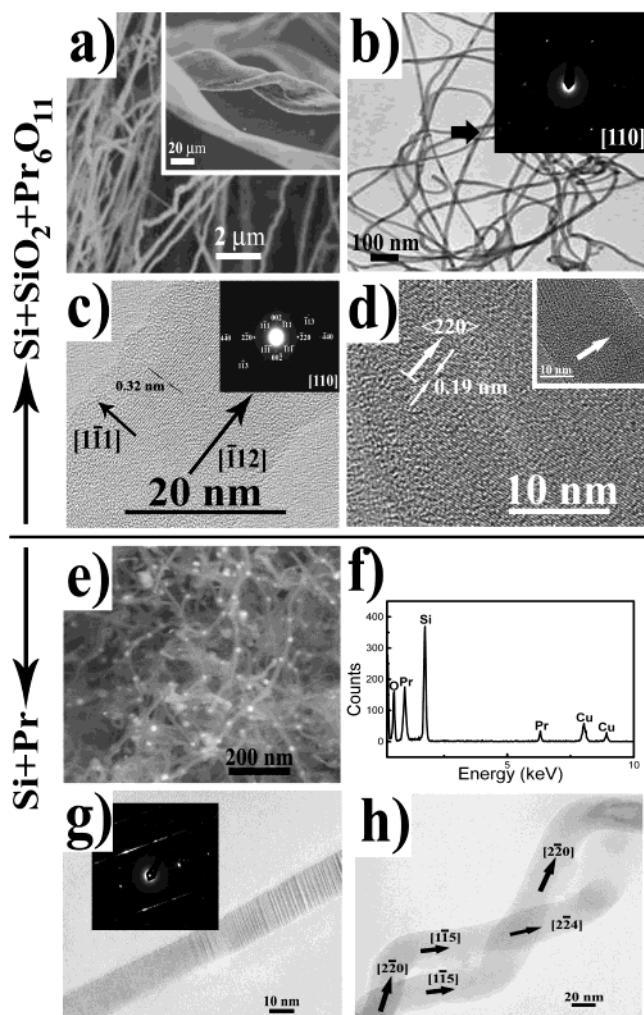
Figure 4. (a) SEM morphology of the SiNWs fabricated from Si + SiO$_2$ + Pr$_6$O$_{11}$, where the diameters of SiNWs are ∼20−30 μm. In addition to the normal SiNWs, helical belts (inset) have also been synthesized with ∼60 μm pitch-length, ∼40 μm belt-width, and ∼3 μm belt-thickness. (b) TEM morphology of SiO$_2$-catalytic SiNWs with a uniform diameter of ∼30 nm. SAED pattern (inset), recorded along the [110] zone axis, for the SiNW (marked by an arrow) indicates that the SiNW is single crystalline. (c) HRTEM lattice image of SiO$_2$-catalytic SiNWs shows the crystalline Si (1$\bar{1}$1) planes with *d*-spacing of 0.32 nm. The [1$\bar{1}$1] crystalline growth axis is perpendicular to the [$\bar{1}$12] wire growth axis. SAED pattern (inset), taken from a spot in the wire-core, shows the coexistence of the {111}, {220}, and {311} lattice plane families. (d) {220} planes have also been observed in SiNWs with *d*-spacing of 0.19 nm. Defects due to micro-twins exist as well. Arrow in the inset points a twin boundary. (e) Pr-catalytic SiNWs have quite uniform diameters of ∼30 nm and contain metal-tips (white spots) which provide evidence of complying with VLS mechanism in the growing process. (f) EDS spectrum indicates the compositions of Si-body and Pr-tip for the SiNWs except the background of O and Cu from the Cu grid used for SEM measurement. (g) Imperfect packings appear in the TEM of Pr-catalytic SiNWs. ED pattern (inset) shows that the SiNW contains quite a few defects of {111} twinnings. (h) TEM morphology of curved SiNWs. The SiNWs change wire-growth directions as indicated, where twinning-defects also show up at the turning sections.

families. This observation was further confirmed by an XRD measurement (not shown). The [1$\bar{1}$1] crystalline growth axis is perpendicular to the [$\bar{1}$12] wire growth axis as indicated by HRTEM and the ED pattern along the [110] zone axis (Figure 4c).

In addition to the Si {111} crystalline planes, {220} planes have also been constructed in SiNWs with *d*-spacing of 0.19
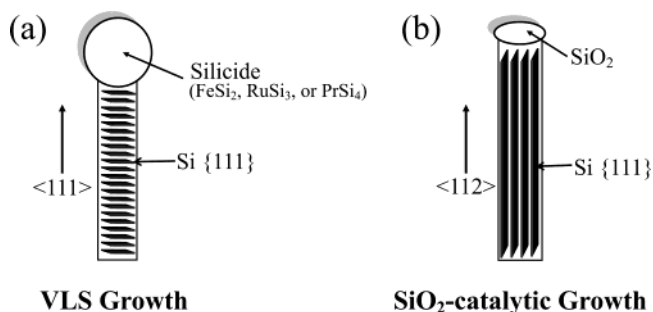

Figure 5. Schematic for the growth models of metal- and SiO$_2$-catalytic SiNWs.
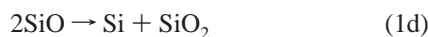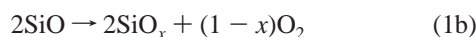
nm (Figure 4d). Such {220} planes, however, appear only occasionally in the crystalline Si cores. Taking a closer look at the magnified HRTEM image (inset of Figure 4d), defects due to micro-twins exist. The micro-twins often locate at the turning section when the growth of SiNW changes direction, consistent with a previous report that micro-twins occur usually in the kinks of SiNWs.[30]

By comparison, the Pr-catalytic SiNWs, as depicted in Figure 4e, are very different in morphology from those catalyzed by SiO$_2$. The Pr-catalytic SiNWs have quite uniform diameters of ∼30 nm, and contain metal-tips (white spots in Figure 4e). These metal-tips again provide an evidence of complying with the VLS mechanism in the growing process. The SEM-EDS shown in Figure 4f indicates the compositions of Si-body and Pr-tip for the SiNWs except the background of O and Cu from the Cu grid used for SEM measurement. The growth direction in the Pr-catalytic SiNWs is the same as those catalyzed by Fe and Ru that the crystalline growth {111} planes are perpendicular to the wire growth axis of ⟨111⟩ as summarized in Table 1.

The twinning-defects, found in the SiO$_2$-catalytic SiNWs (Figure 4d), also appear in Pr-catalytic SiNWs with similar imperfect packings (Figure 4g). The ED pattern in the inset of Figure 4g shows that the Pr-catalytic SiNW contains quite a few defects of {111} twinning, in accordance with a report that the {111} twinning is rather common in the synthesis of Si nanomaterial.[43] Curved SiNWs in Figure 4h are noteworthy. While the SiNWs change their growth directions (Figure 4h), twinning-defects also show up at the same time. If under an ordered alignment, the curved SiNWs could be a prelude for braided SiNWs, like the braided carbon nanofibers reported previously.[44]

3.2. Growth Mechanisms. In our serial experiments for the formation of SiNWs using only pure metal (Fe, Ru, or Pr) as a catalyst, the growth mechanism that we have observed always follows the VLS process. The synthesized SiNW typically has a metal-tip composed of metal and Si, such as FeSi$_2$, RuSi$_3$, and PrSi$_4$, respectively. The crystalline growth axis in all cases is along the ⟨111⟩ direction (Table 1); namely, the most stable {111} plane is perpendicular to the wire growth ⟨111⟩ axis. A schematic for the orientations representing the crystallite and wire growths via VLS mechanism is illustrated in Figure 5a. This result is consistent with the previous studies by Wagner[39] and Lieber and co-workers[21] that a crystalline growth axis of ⟨111⟩ is most favorable in the metal-catalytic fabrications of SiNWs through VLS processes.

In other experiments, we regarded SiO$_2$ as another possible supplying source for Si, thus adding equal weights of Si and SiO$_2$ as reacting samples in the presence of a small amount of metal catalyst (Si/SiO$_2$/metal = 45:45:10%). From chemical point of view, the reduction of SiO$_2$ as a supplier for Si can proceed as

Catalytic Growth of Silicon Nanowires

J. Phys. Chem. B, Vol. 108, No. 3, 2004 **851**

$$Si + SiO_2 \rightarrow 2SiO \tag{1a}$$

$$2SiO \rightarrow 2SiO_x + (1 - x)O_2 \tag{1b}$$

$$SiO_x \rightarrow Si_{1-x} + x(SiO) \tag{1c}$$

$$2SiO \rightarrow Si + SiO_2 \tag{1d}$$

Wire growth direction in the resultant SiNWs, however, is dramatically dependent on whether SiO_2 is included in the reacting sample or not. In all of the cases where SiO_2 exists in the reactants, the $[1\bar{1}1]$ crystalline growth axis in the synthesized SiNWs is perpendicular to the wire axis of $[\bar{1}12]$, i.e., the Si $(1\bar{1}1)$ planes are parallel to the wire axis of $[\bar{1}12]$ (Table 1 and Figure 5b). Besides, the fabricated SiNWs generally have no tips at the wire ends from the reactions containing SiO_2, in sharp contrast to those SiNWs synthesized via VLS mechanism without SiO_2. Occasionally, beadlike nanoparticles/nanoclusters in SiNWs were observed in the SiO_2-containing synthesis (e.g., Figure 2c). The composition for the beadlike nanostructures, however, is mainly SiO_2, opposite to the metal-dominant tips in the SiNWs fabricated without SiO_2. Furthermore, the fabrication reaction with SiO_2 was observed to be able to proceed at a temperature lower than that only using metal and Si as reactants.

SiO_2 has been argued to play a crucial role in the formation of SiNWs by Lee and co-workers,[8,9] who have put forward that SiO_2, acting as a catalyst, is an enhancement ingredient in the growth mechanism of SiNWs. In our serial attempts to examine the effect of SiO_2 on the fabrication of SiNWs, we have also observed the enhancement on the product yield of SiNWs by SiO_2. For the wire crystallization in the SiO_2-catalytic SiNWs in this work, the observed $(1\bar{1}1)$ crystalline planes, parallel to the $[\bar{1}12]$ wire axis, can find support from the study by Dimitriadis et al.[45,46] In the study of Si growth on SiO_2 substrate by chemical-vapor deposition, Dimitriadis et al.[45,46] found that an orientation filtering mechanism, due to the growth-velocity competition in the early stage of growth, is responsible for the preferred orientation of Si films. At the experimental condition of high-pressure silane reactant, the grown Si grains exhibit a strong preferred orientation having Si {111} planes perpendicular to the SiO_2 substrate, as illustrated symbolically in Figure 5b. This result agrees with our observation in the present study, i.e., when SiO_2 acts as a catalyst in the formation of SiNWs, the Si {111} planes extruding from the SiO_2 substrate are perpendicular to the SiO_2 surface (Figure 5b).

3.3. Pressure Effect. To study the size dependence of SiNWs on reacting pressure, three pressure sets of Ar carrier gas, 100, 300, and 500 Torr, have been selected in the synthesis of SiNWs from $Si + SiO_2 + Pr_6O_{11}$. Most of the fabricated nanowires become shorter and wider with increasing Ar carrier pressure as listed in Table 2, indicating while the longitudinal (lengths of SiNWs) growing rate decreases with increasing pressure, the transversal (diameters of SiNWs) one increases.

If under the VLS mechanism, the size of initially formed nanoclusters/nanoparticles is responsible for the diameter of nanowires, such as the $FeSi_2$ liquid-droplet in the Fe-catalytic synthesis of SiNWs. The relation between the diameter of nanoclusters d and the ambient gas pressure p is governed by the inertia fluid model of Yoshida et al.,[47]

$$d \propto p^n, \quad n = \frac{1}{3} \tag{2}$$

From Yoshida's experimental results, they found $n = 1/2.8$ for

TABLE 2: Size Dependence of SiNWs on the Pressure of Ar Carrier Gas[a]

	pressure		
	100 Torr	300 Torr	500 Torr
lengths of SiNWs	tens of μm	several μm	hundreds of nm to several μm
diameters of SiNWs	10–20 nm	~30 nm	30–40 nm

[a] Reaction time is 2 h.

the production of Si nanoparticles by laser ablation with ambient He gas flowing at a constant pressure. Following this model, Zhang et al.[33] also gave similar Ar pressure effect ($n = 1/2.5$) on the growth of SiNWs. Taking our results listed in Table 2 and fitting into eq 2, the dependence ($n = 1/1.72$) of the diameter of SiNWs on the ambient Ar pressure has been determined.

Possible reasons could be found to explain the deviation of our abnormally large $n = 1/1.72$ value from the inertia fluid model by Yoshida et al.[47] First, SiO_2, rather than the metal catalyst, plays a dominant catalytic role in our experiment for the fabrication of SiNWs from $Si + SiO_2 + Pr_6O_{11}$ as discussed in the preceding section. The deviation could stem from a reaction process not complying with the VLS mechanism. Second, a gas-flowing system was employed in our experiment. At higher ambient Ar carrier-gas pressure, the initially formed nanoclusters of Si-grain on SiO_2-substrate are subject to more collisions with Ar atoms, thus slowing down the average drift-velocity of the nanoclusters. Accordingly, the traveling of the nanoclusters takes longer time before their landing on the copper coldfinger or the Si collection-substrate. During this longer period of flight time, bigger sizes of nanoclusters possibly grow, and wider SiNWs are produced consequently.

Meanwhile, the vaporization rate of Si was kept constant under the laser ablation. The absorption/adsorption rate of Si vapor on the nanoclusters of Si-grain on SiO_2-substrate should roughly maintain the same. In a fixed period of time with a constant Si vapor supply, if the SiNW becomes wider, a shorter length of the fabricated SiNW is resulted.

4. Conclusion

We have investigated the growths of crystalline SiNWs with the catalyses of pure metals (Fe, Ru, and Pr) and SiO_2. Si {111} planes have been found to be most stable in these catalytic fabrications. While the wire growth axis is along $\langle 111 \rangle$ for the metal-catalytic SiNWs complying with VLS mechanism, the wire growth axis directs to $\langle 112 \rangle$ in the SiNWs catalyzed by SiO_2. Different growth mechanisms for metal- and SiO_2-catalytic syntheses of SiNWs have been discussed. Pressure effect on the growing process has been examined. Possible reasons have been provided to explain the observations.

References and Notes

(1) Alivisatos, A. P. *Science* **1996**, *271*, 933.
(2) Baron, T.; Martin, F.; Mur, P.; Wyon, C.; Dupuy, M.; Busseret, C.; Souifi, A.; Guillot, G. *Appl. Surf. Sci.* **2000**, *164*, 29.

852 *J. Phys. Chem. B, Vol. 108, No. 3, 2004*

Yang et al.

(3) Park, N.-M.; Kim, S. H.; Sung, G. Y.; Park, S.-J. *Chem. Vap. Deposition* **2000**, *8*, 254.

(4) Liu, H. I.; Biegeisen, D. K.; Ponce, F. A.; Johnson, N. M.; Pease, R. F. W. *Appl. Phys. Lett.* **1994**, *64*, 1383.

(5) Wakayama, Y.; Tanaka, S. *J. Cryst. Growth* **1997**, *181*, 304.

(6) Ono, T.; Saitoh, H.; Esashi, M. *Appl. Phys. Lett.* **1997**, *70*, 1852.

(7) Sanders, G. D.; Chang, Y. C. *Phys. Rev. B* **1992**, *45*, 9202.

(8) Wang, N.; Zhang, Y. F.; Tang, Y. H.; Lee, C. S.; Lee, S. T. *Appl. Phys. Lett.* **1998**, *73*, 3902.

(9) Wang, N.; Tang, Y. H.; Zhang, Y. F.; Lee, C. S.; Lee, S. T. *Phys. Rev. B* **1998**, *58*, 16024.

(10) Wang, N.; Tang, Y. H.; Zhang, Y. F.; Lee, C. S.; Bello, I.; Lee, S. T. *Chem. Phys. Lett.* **1999**, *299*, 237.

(11) Tang, Y. H.; Zheng, Y. F.; Lee, C. S.; Lee, S. T. *Chem. Phys. Lett.* **2000**, *328*, 346.

(12) Zhang, Y. F.; Tang, Y. H.; Wang, N.; Yu, D. P.; Lee, C. S.; Bello, I.; Lee, S. T. *Appl. Phys. Lett.* **1998**, *72*, 1835.

(13) Wang, N.; Tang, Y. H.; Zhang, Y. F.; Yu, D. P.; Lee, C. S.; Bello, I.; Lee, S. T. *Chem. Phys. Lett.* **1998**, *283*, 368.

(14) Zhang, Y. F.; Tang, Y. H.; Wang, N.; Lee, C. S.; Bello, I.; Lee, S. T. *J. Cryst. Growth* **1999**, *197*, 136.

(15) Tang, Y. H.; Zhang, Y. F.; Wang, N.; Shi, W. S.; Lee, C. S.; Bello, I.; Lee, S. T. *J. Vac. Sci. Technol. B* **2001**, *19*, 317.

(16) Lee, S. T.; Zhang, Y. F.; Wang, N.; Tang, Y. H.; Bello, I.; Lee, C. S.; Chung, Y. W. *J. Mater. Res.* **1999**, *14*, 4503.

(17) Fan, X. H.; Xu, L.; Li, C. P.; Zheng, Y. F.; Lee, C. S.; Lee, S. T. *Chem. Phys. Lett.* **2001**, *334*, 229.

(18) Shi, W. S.; Peng, H. Y.; Zheng, Y. F.; Wang, N.; Shang, N. G.; Pan, Z. W.; Lee, C. S.; Lee, S. T. *Adv. Mater.* **2000**, *12*, 1343.

(19) Zhang, Y. F.; Tang, Y. H.; Lam, C.; Wang, N.; Lee, C. S.; Bello, I.; Lee, S. T. *J. Cryst. Growth* **2000**, *212*, 115.

(20) Li, C. P.; Sun, X. H.; Wong, N. B.; Lee, C. S.; Lee, S. T.; Teo, B. K. *Chem. Phys. Lett.* **2002**, *365*, 22.

(21) Morales, A. M.; Lieber, C. M. *Science* **1998**, *279*, 208.

(22) Hu, J.; Odom, T. W.; Lieber, C. M. *Acc. Chem. Res.* **1999**, *32*, 435.

(23) Duan, X.; Lieber, C. M. *J. Am. Chem. Soc.* **2000**, *122*, 188.

(24) Cui, Y.; Leiber, C. M. *Science* **2001**, *291*, 851.

(25) Hu, J.; Ouyang, M.; Yang, P.; Lieber, C. M. *Nature* **1999**, *399*, 48.

(26) Cui, Y.; Lauhon, L. J.; Gudiksen, M. S.; Wang, J.; Lieber, C. M. *Appl. Phys. Lett.* **2001**, *78*, 2214.

(27) Yu, D. P.; Lee, C. S.; Bello, I.; Sun, X. S.; Tang, Y. H.; Zhou, G. W.; Bai, Z. G.; Feng, S. Q. *Solid State Commun.* **1998**, *105*, 403.

(28) Yu, D. P.; Bai, Z. G.; Ding, Y.; Hang, Q. L.; Zhang, H. Z.; Wang, J. J.; Zou, Y. H.; Qian, W.; Xiong, G. C.; Zhou, H. T.; Feng, S. Q. *Appl. Phys. Lett.* **1998**, *72*, 3458.

(29) Feng, S. Q.; Yu, D. P.; Zhang, H. Z.; Bai, Z. G.; Ding, Y. *J. Cryst. Growth* **2000**, *209*, 513.

(30) Zhou, G.; Zhang, Z.; Yu, D. P. *J. Cryst. Growth* **1999**, *197*, 129.

(31) Yu, D. P.; Bai, Z. G.; Wang, J. J.; Zou, Y. H.; Qian, W.; Fu, J. S.; Zhang, H. Z.; Ding, Y.; Xiong, G. C.; You, L. P.; Xu, J.; Feng, S. Q. *Phys. Rev. B* **1999**, *59*, 2498.

(32) Zhou, G. W.; Zhang, Z.; Bai, Z. G.; Feng, S. Q.; Yu, D. P. *Appl. Phys. Lett.* **1998**, *73*, 677.

(33) Zhang, H. Z.; Yu, D. P.; Ding, Y.; Bai, Z. G.; Hang, Q. L.; Feng, S. Q. *Appl. Phys. Lett.* **1998**, *73*, 3396.

(34) Bai, Z. G.; Yu, D. P.; Wang, J. J.; Zou, Y. H.; Qian, W.; Fu, J. S.; Feng, S. Q.; Xu, J.; Lou, L. P. *Mater. Sci. Eng. B* **2000**, *72*, 117.

(35) Xing, Y. J.; Yu, D. P.; Xi, Z. H.; Xue, Z. Q. *Chin. Phys.* **2002**, *11*, 1047.

(36) Xing, Y. J.; Xi, Z. H.; Yu, D. P.; Hang, Q. L.; Yan, H. F.; Feng, S. Q.; Xue, Z. Q. *Chin. Phys. Lett.* **2002**, *19*, 240.

(37) Yan, H. F.; Xing, Y. J.; Hang, Q. L.; Yu, D. P.; Wang, Y. P.; Xu, J.; Xi, Z. H.; Feng, S. Q. *Chem. Phys. Lett.* **2000**, *323*, 224.

(38) Wagner, R. S.; Ellis W. C. *Appl. Phys. Lett.* **1964**, *4*, 89.

(39) In *Whisker Technology*; Levitt, A. P., Ed.; Wiley-Interscience: New York, 1970; pp 47−119.

(40) Seddon, E. A.; Seddon, K. R. *The Chemistry of Ruthenium*; Elsevier: Amsterdam, 1984.

(41) Harris, D. C. *Quantitative Chemical Analysis*, 4th ed.; W. H. Freeman and Company: New York, 1995.

(42) Ishida, S.; Iwamoto, Y.; Kabuto, C.; Kira, M. *Nature* **2003**, *421*, 725.

(43) Ma, X. L.; Zhu, Y. L.; Zhang, Z. *Philos. Mag. Lett.* **2002**, *82*, 461.

(44) Boehm, H. P. *Carbon* **1973**, *11*, 583.

(45) Dimitriadis, C. A.; Stoemenos, J.; Coxon, P. A.; Friligkos, S.; Antonopoulos, J.; Economou, N. A. *J. Appl. Phys.* **1993**, *73*, 8402.

(46) In *Silicon-Based Materials and Devices*; Nalwa, H. S., Ed.; Academic Press: San Diego, 2001; Vol. 2, pp 193−223.

(47) Yoshida, T.; Takeyama, S.; Yamada, Y.; Mutoh, K. *Appl. Phys. Lett.* **1996**, *68*, 1772.